

# **Real-time Detection of Oil Slick Thickness Patterns with a Portable Multispectral Sensor.**

Final Report  
Submitted to the U.S. Department of the Interior  
Minerals Management Service  
Herndon, VA  
July 31, 2006

Contract No. 0105CT39144



**Principal Investigator:** Dr. Jan Svejksky, Ocean Imaging Corp. 201 Lomas Santa Fe Dr.,  
Suite 370, Solana Beach, CA 92075 (858) 792-8529, Fax: (858) 792-8761, [jan@oceani.com](mailto:jan@oceani.com)

**Co-Investigator:** Judd Muskat, CDFG Office of Oil Spill Prevention and Response, 1700 "K"  
Street, Sacramento, CA 95814 (916) 324-3411, [JMuskat@dfg.ca.gov](mailto:JMuskat@dfg.ca.gov)

## **Acknowledgement**

This project was funded by the U.S. Minerals Management Service. The authors wish to thank the U.S. Minerals Management Service, Engineering Branch for funding this study and Joseph Mullin for his guidance in the work. Thanks also go to the California Department of Fish and Game, Office of Oil Spill Prevention and Response for providing the plane and pilot for the remote sensing experiments over the Santa Barbara, CA oil seeps, to Mr. Merrill Jacobs and Mr. Rick Gill of Clean Seas LLC, Carpinteria, CA for providing the vessels and crew to assist in the sampling of the Santa Barbara, CA oil seeps and to the staff of the Ohmsett Facility for their assistance in the remote sensing overflights.

## **Disclaimer**

This report has been reviewed by the U.S. Minerals Management Service staff for technical adequacy according to contractual specifications. The opinions, conclusions, and recommendations contained in the report are those of the author and do not necessarily reflect the views and policies of the U.S. Minerals Management Service. The mention of a trade name or any commercial product in the report does not constitute an endorsement or recommendation for use by the U.S. Minerals Management Service. Finally, this report does not contain any commercially sensitive, classified or proprietary data release restrictions and may be freely copied and widely distributed.

**On the Cover:** Clean Seas vessel being guided into an oil slick by the aircraft imaging crew over the Santa Barbara Channel seeps.

## **EXECUTIVE SUMMARY**

This project aimed to develop an algorithm that would enable the measurement of oil slick thicknesses using multispectral aerial imagery in the UV-Visible-NearIR spectral range. Using an existing 4-channel sensor the project was also designed to evaluate the feasibility of developing a relatively economical, portable aerial oil spill mapping system that could be operationally deployed. Such a system would enable rapid mapping of the extents and thicknesses of an oil spill with greater quantitative and geographical accuracy than is presently possible using visual observations. Using data obtained under small-scale laboratory conditions, larger-scale experiments at Ohmsett – The National Oil Spill Response Test Facility in Leonardo, New Jersey, and aerial and ship-based field sampling of slicks from natural oil seeps in California’s Santa Barbara Channel a working oil thickness algorithm was developed for medium weight crudes and IFO-180 fuel oil. The algorithm is adaptive in that it estimates oil thickness using spectral reflectance deviations from existing water color background characteristics, thus allowing it to be applied in different geographical areas with different water color conditions. The algorithm can measure film thicknesses between sheens and approximately 0.4-0.5mm. The range could potentially be extended by adding an infrared sensor to the system.

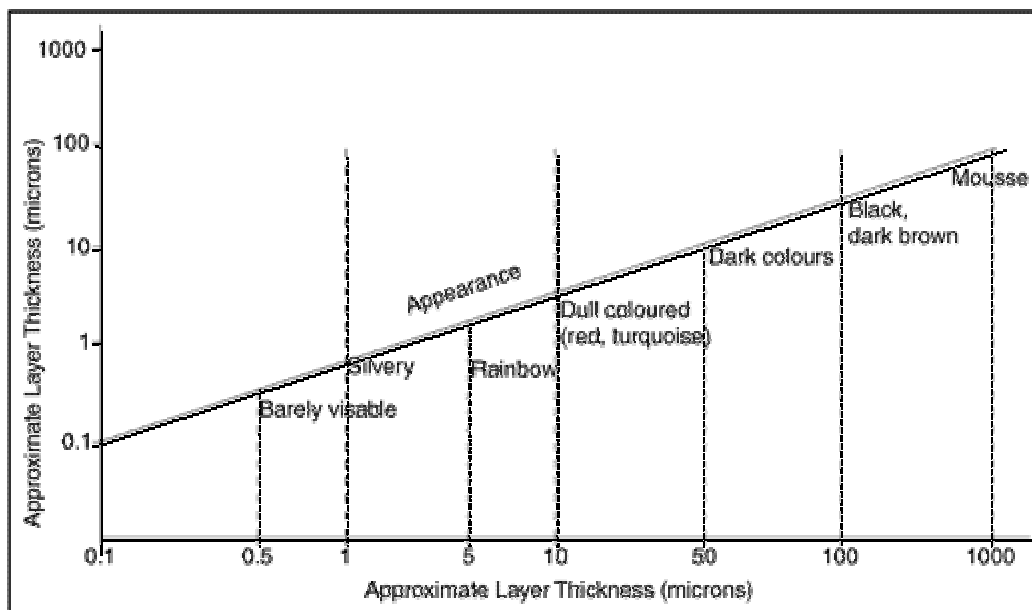
The project proved that the development and operational utilization of a portable multispectral imaging system for oil spill mapping is very feasible and could provide major improvements in oil spill response. Further development, which could not be accomplished during this project’s 18-month timeline, includes improvements in hardware and software that will allow better autogeolocation and processing of the data in near-real-time, integration of an IR camera with the system for increased thickness detection range, and acquisition of additional oil signature profiles under different atmospheric conditions.

# 1. PROJECT BACKGROUND

## 1.1 Present-day Oil Spill Assessment Techniques

One of the most important initial steps in response to an oil spill at sea is the assessment of the extents of the oil slick and the quantity (i.e. thickness) distribution of oil within it. Since many types of hydrocarbons rapidly spread out to very thin layers when released at sea, accurate determination of which areas contain the most amount of oil is vital for efficiently guiding oil spill response efforts. Addages often mentioned by response crews such as “80% of the oil is contained in 20% of the slick” and “wasting time chasing sheens” illustrate the common, frustrating problem of misallocating time and resources due to insufficient knowledge of the oil thickness distribution within a spill.

The vast majority of oil quantity distribution assessments are presently done visually from helicopter or aircraft. Figure 1. shows thickness guidance parameters based on oil film appearance, which are commonly included in oil spill response training guides throughout the world. Such visual observations from aircraft (sometimes supplemented by drawings or digital photographs) suffer from three main complications. First, any verbal, graphic or oblique photographic documentation is usually based only on approximate geolocation information obtained through the aircraft’s GPS. Even if it is later reformatted as input into a computerized Geographical Information System (GIS), the data can contain a great degree of positional error. Second, visual estimation of oil film thickness distribution is highly subjective, is affected by varying light and background color conditions and, if not done by specially trained and experienced personnel, tends to be inaccurate. Most often the observers’ tendency is to overestimate the amount of oil present. Third, comprehensive visual assessments are impossible at night.



(Courtesy CONCWE, A Field Guide to the application of dispersants to oil spills)

Figure 1. Oil-on-water appearance related to its thickness for guiding visual assessments. (Ref. 11)

## 1.2 Remote Sensing Methodologies

Satellite and aerial remote sensing can, in principle, provide a convenient means to detect and precisely map marine oil spills, and provide timely information for guiding recovery operations. Significant advances have been made (primarily in Europe and Canada) in oil spill detection capabilities, and side-looking airborne radar and infrared/ultraviolet detectors are being used operationally in Europe. Recently, a sophisticated airborne laser fluorosensor and microwave radiometer for measuring oil thickness have been added to two operational marine surveillance aircraft in Germany (1). Despite this, visual observations continue to be the dominant oil spill distribution assessment method used throughout the world.

Satellite sensors with resolution adequate for oil slick detection have a number of disadvantages for their routine use in spill monitoring. These include low revisit frequency (2-6x/month), relatively low spatial resolution, high cost, and high false target occurrence. Satellite-borne synthetic aperture radars (SARs) provide only minimal ability to measure relative thickness of oil slicks. Likewise, multifrequency/multipolarization aerial SARs have shown poor ability to discern oil-on-water thickness (2,3). Some researchers have found correlations between oil thickness and its reflective properties detected by multispectral satellite imagers but the poor revisit frequency, cloud cover problems and, in most cases, lack of real-time data delivery infrastructure make such instruments ineffective for operational utilization.

Research of oil thickness detection using aerial instruments has focused primarily on active optical and acoustic techniques using lasers (4,5). After much development, some promising results were achieved with the highly complex LURSOT system (6). This instrument uses a high energy laser to heat the surface of the oil slick and another, precisely aligned probe laser to detect the thermal displacement. A Doppler shift measurement of the probe beam is then used to compute thickness of the slick. If it is ever successfully deployed, the LURSOT's uniqueness and bulk makes it primarily a research system not suitable for rapid-deployment operational use. Some positive results have also been achieved with aerial infrared (IR) imagers. For reasons not yet clearly understood, thick oil appears warmer than water and intermediate thickness oil appears cooler. The thickness at which the warm-to-cool transition occurs is not sharply defined, however, and thus limits measurement accuracy. This deficit and the inability to detect oil sheens limits IR sensors' operational usefulness. Laser fluorosensors have also shown some promise in oil thickness detection, most notably instruments utilizing Raman scattering principles (7). As is mentioned above, Germany has begun to use them operationally in two aircraft. However, since the maximum altitude at which laser instruments can be flown is 500-600', the resulting spatial coverage is extremely narrow. Operational use aiming to map the spatial distribution of thicknesses within an oil slick requires flying a grid of closely spaced flight lines covering the entire region within which the presence of oil is suspected – which may be impractical in many instances. (A scanning laser fluorosensor which offers an "image" swath of 50-100m was recently developed in Canada at a cost of several million dollars.) Additionally, the Raman signal can only be used to measure relatively thin oil films of 10  $\mu\text{m}$  or less since it disappears over thicker oil accumulations (13).

The potential utilization of relatively low-cost UV-Visible-nIR aerial imagers for oil thickness mapping has, in our opinion, not been adequately investigated in the past. Although sometimes matter-of-factly dismissed (usually based on results obtained with now-obsolete instruments available in the 80s and early 90s), recent research suggests that oil thickness detection algorithms can be developed using new high radiometric resolution (e.g. 12-bit) multispectral data recently available from relatively economical, portable instruments. Since these instruments also provide DGPS-geolocated images, analyses synoptically covering large areas of the sea surface can be immediately disseminated in GIS-compatible format to ground crews via a satellite phone data link. This project aimed to develop and evaluate the utility of such an oil thickness sensor stressing portable, operational application.

## **2. PROJECT OBJECTIVES**

Oil pollution recognition programs such as the European Union's DISMAR represent multi-nationally funded projects with adequate funding to equip an entire fleet of dedicated aircraft with specialized oil-sensing instruments. No such program of similar magnitude presently exists in the United States. Additionally, while the European efforts primarily focus on the North Atlantic region surrounding Europe, the U.S. and neighboring countries must deal with areas of much larger proportions in two widely separated oceans. The availability of one or even several detection instruments in dedicated aircraft within North America thus does not present a practical monitoring solution for rapid response in most oil spill incidents. In most cases, local Coast Guard and/or spill response agency aircraft are mobilized to aid in response planning and recovery.

An economical, portable and easy-to-operate oil slick detection and thickness measurement instrument which could be regionally owned and operated would provide the needed technology. Optical sensors are one logical choice. Such instruments are relatively affordable to state agencies and local contractors, are usually very portable, and can be rapidly mounted and deployed in a variety of aircraft. This makes them ideal for widespread operational use.

This project aimed to begin development of such a sensor by utilizing Ocean Imaging's (OI's) existing instrument as the imaging platform. OI owns and operates the DMSC-MKII aerial imager, manufactured by SpecTerra Ltd. in Australia. The DMSC is a portable, 4-channel sensor with 12-bit radiometric resolution. It's channels can be customized for any wavelength between approximately 400nm (UV) and 950nm (near-IR).

Simplicity, portability and ease-of-use under real-world, operational conditions were paramount in guiding the development phases of this project. In its simplest terms, our aim was to develop an automated, computerized system that will utilize similar oil thickness-related color differences as are presently being exploited with visual

observations – but map the thickness distributions with greater objectivity and spatial accuracy.

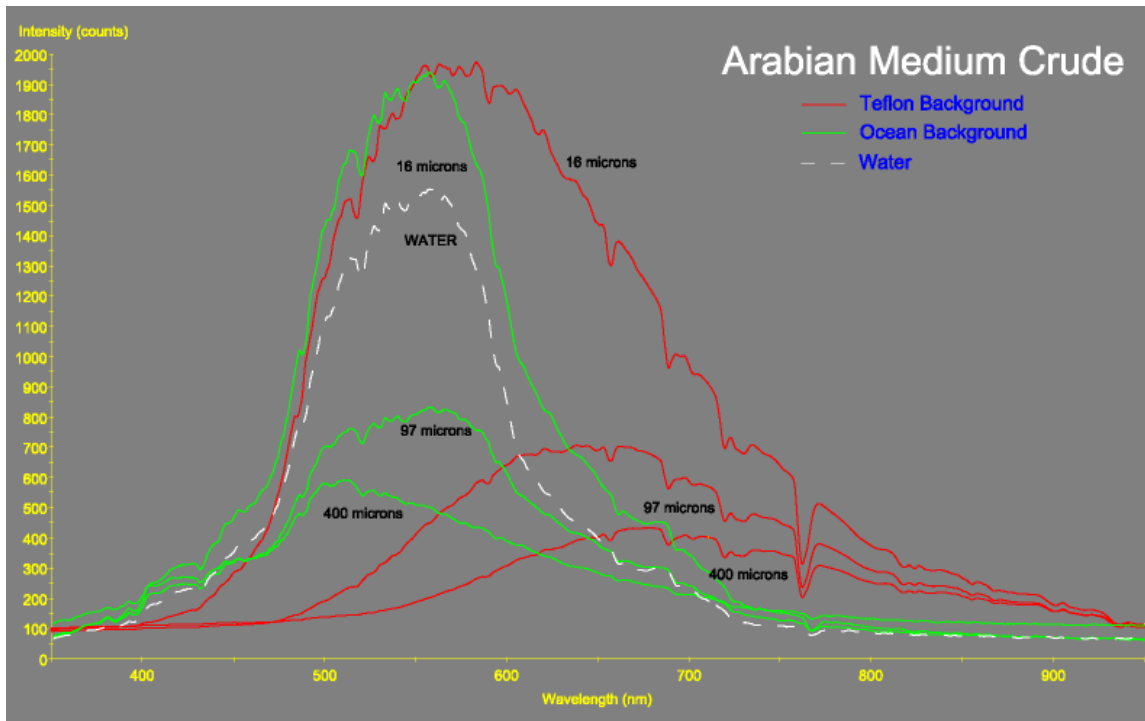
The project had three distinct phases: 1) development of the thickness measurement algorithms; 2) refinement of the algorithms using real-world imagery and field-sampled thickness measurements over natural oil seeps in the Santa Barbara Channel, California; 3) final algorithm validation under controlled conditions at Ohmsett – The National Oil Spill Response Test Facility in Leonardo, New Jersey. The final goal was to incorporate the developed algorithms into a pseudo-operational system capable of imaging a spill, create a thickness distribution map and disseminate it to ground crews in near-real-time. All phases of the project were completed successfully, although the Ohmsett experiments revealed several late-stage algorithm refinement needs (described below in the “Ohmsett Experiments section”) that could not be tested for previously. At the termination of the 18-month project, the image acquisition-to-thickness map-dissemination timeline is 2-3 hours, although this lag can be substantially decreased with further software development.

### **3. RESULTS**

#### **3.1 Algorithm Development**

This project’s premise for developing an oil thickness measurement algorithm using multispectral imagery was that it be as universal as possible to allow operational use in different geographic regions and under different oceanic and atmospheric conditions. To satisfy this requirement we recognized four important variables that could be expected to affect the algorithm’s outcome: 1) oil type; 2) differences in background water color; 3) differences in illumination (sun angle and sunny vs. cloudy conditions); 4) lack of field measurements or other in-situ data that would allow site-specific algorithm calibration. Previous published research in utilizing multispectral imagery for oil thickness determination generally used one of two approaches: multispectral classification where the resulting classes were calibrated for thickness using some external or in-situ data (5,9,10), or the computation of ratios between specific wavelengths and relating the ratio values to oil thickness through laboratory testing (10,12). Unfortunately, the researchers tended to ignore variability due to background water color or illumination (most studies do not even mention whether the data were gathered under sunny or cloudy conditions), and their results tend to be very specific for each particular experiment. This makes the previous studies of little use in applying them to the development of a real-world, operational system. Our own spectrometric measurements, shown in Figure 2, illustrate how strongly the reflectance spectra of thin oil films are attenuated by the underlying water spectral signature.

In view of the relatively short time-span of this project, we decided to place certain constraints on the above variables to facilitate the initial algorithm development. We limited the types of oil to unrefined crudes (some tests were also done with IFO-180 bunker fuel later in the project). The justification was that crude oils and bunker fuels tend to be of more concern in oil spill situations than more volatile hydrocarbons such as



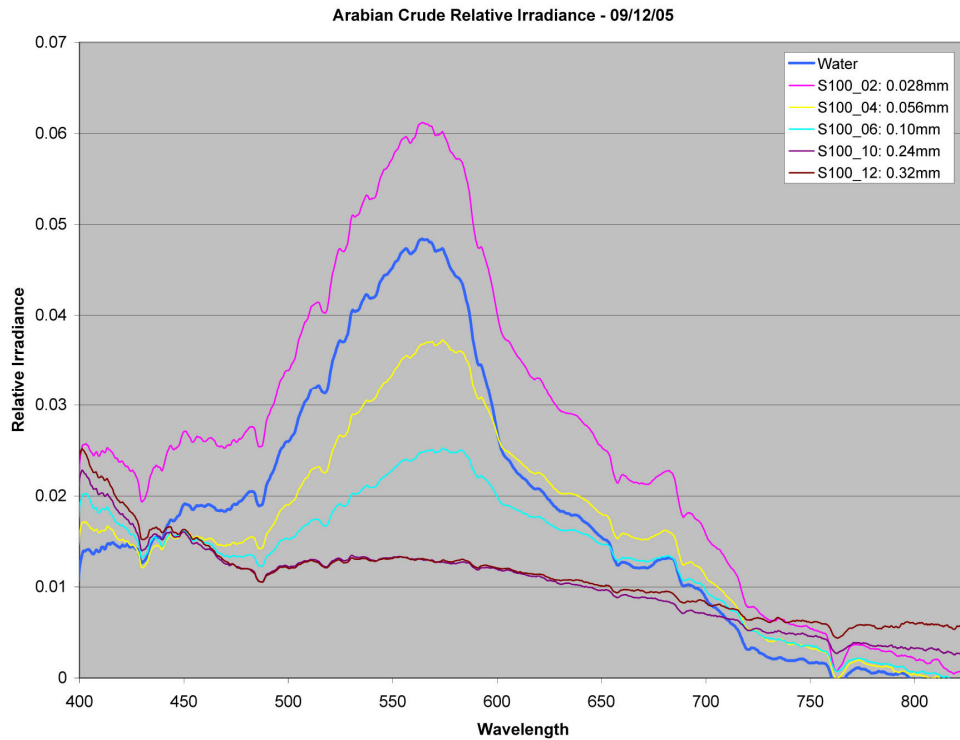
**Figure 2.** Spectrometer measurements of Arabian Medium Crude films of several thicknesses over an evenly reflecting background (red) and deep coastal ocean water (green). Note the major shift toward shorter wavelengths caused by attenuation by the background water signal.

diesel and gasoline which are often simply allowed to evaporate. Additionally, our planned at-sea experiments in the Santa Barbara Channel would involve Monterey Crude – a relatively heavy crude oil. Another initial constraint was that the algorithm be developed for sunny conditions, with the understanding that a modified version for oil thickness determination under cloudy weather be added later in the project.

### 3.2 Laboratory Tests

Early in the project OI obtained from the Ohmsett test facility several samples of crude oils for experimentation. These included Arabian Medium Crude, “Rock” (a heavier crude similar to Monterey), and IFO-180. Later, additional samples of Alaska North Slope Crude and Northstar crude oil were also obtained and tested. To study the oils’ reflectance characteristics, which would guide the choice of wavelengths to use in the algorithm, OI used a portable spectrometer to capture reflectance spectra of different oil films of known thicknesses. In order to approximate real-world conditions (i.e. oil on deep water) the films were created by placing known amounts of oil in an optically clear glass vessel partially filled with sea water and partially submerged in a deep water harbor. The spectrometer probe was then placed vertically above the container and the spectrum was recorded. Thicker films were achieved by adding sequentially greater amounts of oil into the container. Upon completion of each thickness sequence all the oil in the vessel was recovered for proper disposal. Figure 3 shows sample results for





**Figure 3.** Reflectance spectra of Arabian Medium Crude films of various thickness over deep water background in Oceanside Harbor, California. (Note that very thin films actually cause a slight increase in surface reflectance from the clear water/background spectrum.)

various Arabian Crude thickness films. The spectrometer experiments resulted in several conclusions:

- No specific or unique reflectance/absorbance peak exists at any wavelength that distinctly changes with oil thickness
- Under real-world conditions (i.e. deep water reflectance attenuates the overlying oil signal) the greatest reflectance changes due to thickness variations occur in spectral ranges between 400 - 480 and 620-680nm
- At film thickness greater than approximately 0.2mm for light and medium crudes and 0.1-0.15 for heavy crudes the background water reflectance signal is no longer a significant factor since all detected reflectance originates within the oil film itself.
- For films over deep water (i.e. no bottom reflectance) very little spectral change was measured for Medium Crude films thicker than approximately 0.5mm, indicating this may be the upper thickness detection limit of an algorithm solely based on UV-Vis-NearIR wavelengths.

- Very low oil reflectance occurs in the near-IR range at most thicknesses.

This last finding appeared to contradict several previously published studies which utilized imagery in the near-IR range for their thickness determinations (6,8,9). Due to this, we initially assumed that our low reflectance readings in the near-IR region were caused by a sensitivity fall-off of the spectrometer. Additional experiments done at our lab by floating oil films in 6-8" deep water-filled translucent pans placed over a blue-green background (to simulate water color) and imaged with the actual DMSC sensor appeared to corroborate the previously published research and validate the value of near-IR wavelengths for oil thickness determination. As will be explained in the "Ohmsett Experiments" section below, our initial spectrometer measurements ultimately proved correct, since the increased near-IR signal in our (and perhaps other researchers') laboratory experiments were due to artificial reflectance from the bottom of the insufficiently deep pans.

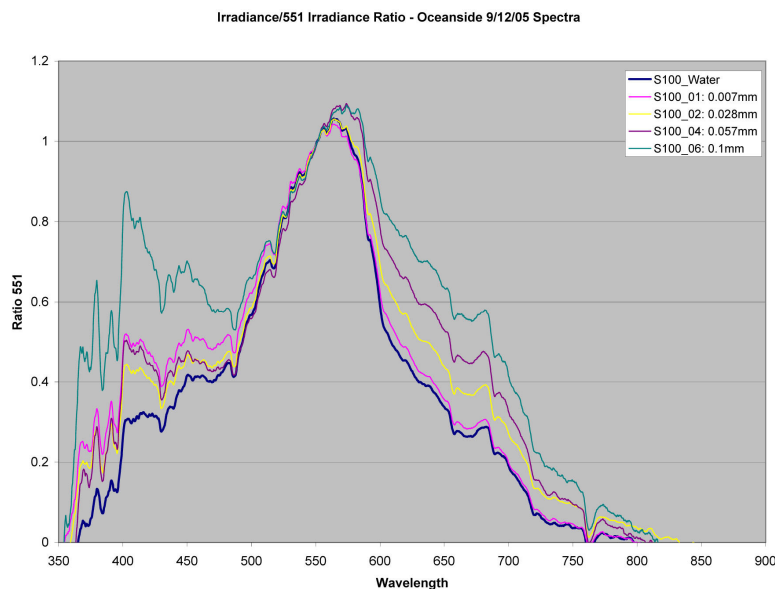
Our spectrometer studies and subsequent software tests confirmed that neither of the previously published approaches – multispectral classification or simple use of band ratios – can be successfully used to develop an operational oil thickness mapping algorithm. This is primarily because at film thicknesses of 0.2mm or less (which dominate an oil slick in most incidents) the underlying water color reflectance effects vary with location or oceanic conditions and thus alter the classification or ratio results in an unpredictable manner. Instead, we developed the following thickness determination algorithm approach: When imaging an oil spill with the multispectral aerial sensor, a nearby area of the ocean not contaminated with oil is also imaged. Ratios between the individual wavelength channels are then computed for both the known clear water area and all other pixels. The thickness determination is based on the deviation of each available ratio from the "clear water ratio" for the same pair of wavelengths. Since multiple ratios are available with the 4-channel DMSC, the deviations between ratios can be further utilized to establish a thickness measurement for each oil-contaminated pixel. The actual algorithm utilizes a fuzzy ratio-based classification to assign each pixel into a thickness range. The algorithm and software running procedure are described in more detail in Appendix 1. The fuzzy classification utilizes "oil signature files" which contain experimentally-derived or field-derived archived information about specific oil types, ocean condition effects, etc.

We believe our algorithm approach has several important advantages over other researchers' approaches. First, it takes into account the effects of the existing water color background and determines thickness based on radiometric deviations from this background – thus making it more universally applicable. Second, by using stored information in individual "oil signature files" the software routine can be readily expanded to contain new parameters. For example, if the general type of oil spilled is known, the signature file containing thickness-related information for that oil type can be used for best accuracy. Similarly, different signature files can be applied under "sunny" and "cloudy" image acquisition conditions. As the project continued, we expanded the signature file library to make the algorithm instantly customizable for different oil types

and ocean conditions (e.g. using data obtained during the Santa Barbara Channel experiments).

As part of the image acquisition, radiometric calibration data are collected to allow standardized calibration of the image data (so that archived thickness information stored in the signature files is applicable to each new image set), and to correct succeeding portions of the data set for sun angle (i.e. time of day) variability. This is done using a procedure developed, tested and routinely utilized by OI prior to this project. It uses DMSC measurements of a white Teflon reflector imaged on the ground before and after the flying mission, and periodic Teflon reflectance readings obtained with a portable spectrometer while in flight.

A somewhat surprising conclusion after much lab experimentation and tests done over the Santa Barbara Channel seeps was that the choice of specific wavelengths for the DMSC's 4 channels to maximize thickness detection capability is not as stringent as we had initially assumed. The reason is illustrated in Figure 4. The Figure shows full spectra of Arabian crude over deep water, expressed as the ratio of each wavelength to 551nm – the wavelength of one of our filters closest to the maximum reflectance of the clear water signal. The data indicate that the greatest thickness-related reflectance changes occur in the 400-480nm (UV-blue) range, and approximately 625-680nm (orange-red) range. Within those ranges, however, the thickness-related change in reflectance (and hence the ratio) is relatively constant. (Note that in the 400-480nm range the ration first decreases then increases due to affects of the film's thickness on its fluorescence emission.) Hence as long as the multispectral sensor is loaded with at least one channel within each range plus one within the peak reflectance range the algorithm has enough information available for thickness differentiation (provided, of course, that the stored signature files contain information gathered at the same wavelengths).



**Figure 4.** Reflectance ratios relative to 551nm of Arabian Medium Crude over deep water (see text for discussion).

### 3.3 Santa Barbara Oil Seep Experiments

#### 3.3.1 Experiment Overview

The primary objective of the Santa Barbara experiments was to obtain simultaneous oil slick multispectral aerial imagery and slick thickness measurements at known locations from a sampling vessel. The data collection was done on the morning of two days - 12 and 13 October, 2005. Multiple thickness and image samples were obtained at four separate slicks on the first day and two slicks on the second day. Although most of the thicker oil slicks found in the S. B. Channel tend to be weathered, one of the slicks sampled on 10/13 was composed of relatively fresh, thick oil. Our collected data thus include weathered, emulsified as well as fresh, very liquid samples. Enough samples were collected so that some were used for calibrating the multispectral thickness algorithm while others were retained for validation purposes.

**Coordination Logistics:** Each morning the participants divided into two teams - an aircraft team and a boat team. The two communicated via aeronautical frequency radio. Vessels provided by Clean Seas transported the field crew to the region off Coal Oil Point west of Santa Barbara. That area has two of the largest active seeps and was thus chosen for its great probability of encountering sizable oil slicks. Once in the vicinity, the aircraft team (using a Partenavia Observer owned by CDFG) took off from Santa Barbara, surveyed the area and verbally directed the sampling vessel to a desirable slick. Since many of the existing slicks are extremely thin, the selection criteria were primarily based on locating areas of thicker ( $>0.1\text{mm}$ ) oil films. The air-boat verbal communication/direction worked very well and the aircraft team successfully guided the sampling vessel to areas of homogeneously distributed oil of various thicknesses. Once on station, the field crew began taking thickness samples while the air crew imaged the area several times from different directions (to provide data on the possible effects of sun/viewing geometry on the measurements). The vessel crews also collected spectrometer readings of a teflon target, used for calibrating the DMSC imagery. (The calibration accounts for changing light levels during the day due to changing sun angle.).

**Thickness Sampling Considerations:** Prior to the field experiments, the Ocean Imaging team experimented with several published methods for sampling oil film thickness. Tests were done in the lab (where the exact amount of oil to be recovered was known *a priori*), and in the field during a previous boat trip in the Santa Barbara Channel. We settled on the following procedure, based on accuracy as well as practicality for quick, in-the-field measurements: A plexiglass plate is cleaned thoroughly with degreasing solvent and wiped dry. The plate is then partially vertically submerged through the oil film and drawn back up. The oil's strong adherence properties cause the film to stick to the plate and, as the plate is being submerged, continue to draw surrounding film onto the plate. The same adhesion process continues as the plate is drawn back up through the film. When retrieved on-board, each side of the plate thus contains collected oil film from twice its total surface area. The collected oil is carefully scraped off into an appropriate sized syringe, air is displaced and the oil volume is measured. From this and the measurement of the plexiglass area that was submerged, the oil film thickness can be computed.



**Figure 5.** The oil thickness sampling plate being lowered into a Santa Barabara Channel oil slick (left); The same plate after being raised from the slick (right).

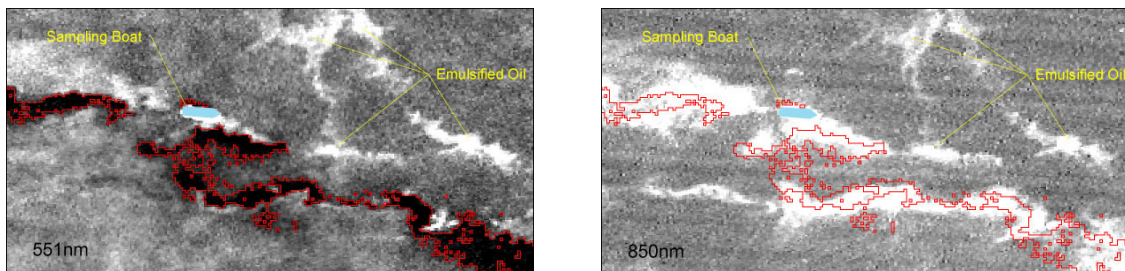
To alleviate concerns that the boat itself may alter the film's thickness by aggregating it as it drifts through, we did not collect any samples on the down-drift side of the vessel and, on the second day, attached the collection plates to a 6 foot boom so the samples were taken away from the hull.

During each sampling process we watched carefully that the oil film does indeed adhere continuously to the plate. We found that fresh oil films and the thicker aged or emulsified films consistently adhere to the plate as it is being submerged and again as it is drawn upward through the film. This tended to not be the case with very thin ( $<0.005\text{mm}$ ) aged films which tend to have a "crusty" characteristic. In their case, the oil was drawn onto the plate as it was being submerged but the film broke as the plate began to be withdrawn and did not adhere completely in the up direction. For this reason, when taking such thin film samples, we cleared any surrounding film from around the plate after submerging it and quickly withdrew it through the clean water. The amount of oil on each side of the plate was then assumed to represent film covering only one equivalent of the area of the submerged plate. Photos illustrating the procedure are shown in Figure 5. We realize that no perfect oil thickness sampling method exists and ours also was not error-free. However, we believe that the error margins achieved are acceptable in view of the main objectives of the project.

### 3.3.2 Experiment Results

Imagery from each sampling site was preprocessed (georeferenced, radiometrically calibrated using the preflight and in-flight Teflon spectra, corrected for vignetting effects and mosaicked) and run through our oil-detection neural network routine to identify potential areas with oil on the ocean surface and mask non-oil-affected areas. Since imagery was obtained multiple times over each site from different directions (i.e. sun/viewing angles) the robustness of the routine could be tested in relation to various flight geometry parameters. We achieved very consistent results.

Next, various ratios between the 4 DMSC channels were computed for the areas containing oil and open water. Being still believers at the time in the potential value of the near-IR region of the spectrum for oil thickness determination, we concentrated on the 600nm-to-nearIR range for creating signature files from approximately half of the data sets. Curiously, the near-IR (850nm) channel proved quite useful for both, training the algorithm and testing its accuracy with the other half of the data set. The reason for this, as we determined later, was because most of the oil signal in the acquired imagery represented aged or emulsified oil. We found the process of weathering to dramatically alter the oil's reflectance characteristic in the near-IR, causing it to become strongly reflective in that spectral region. This property is illustrated in Figure 6. The observed effect can be exploited to provide an additional, important capability of our remote sensing system: the ability to identify and differentiate between weathered/emulsified and fresh oil areas based on differences in reflectance response between 550nm and near-IR (e.g. 850nm) channels. Thus while a near-IR channel does not contribute significantly to thickness determination of fresh oil films, it should be included on the imager if the presence of oil emulsions is of concern.

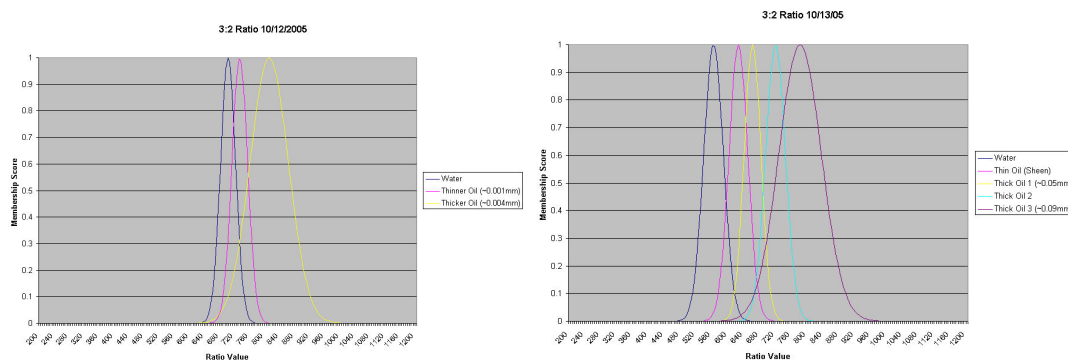


**Figure 6.** DMSC image of oil seep area containing both weathered and fresh oil. Note that while the 850nm (near-IR) channel recorded strong reflectance only from areas that contained only weathered oil or a mixture of both types, the 551nm channel response shows strong differentiation between weathered oil (high reflectance) and fresh oil (strong absorbance).

We also speculated that variations in the background reflectance (i.e. clean water leaving radiance and atmospheric effects) will sufficiently attenuate the oil signal so that a simple, universal relationship of the various ratios to oil slick thickness will not be attainable. This experiment's data provided insights into the background reflectance-caused variability. The first experiment day began with foggy weather and the skies cleared sufficiently by mid-morning for the plane to begin imaging. There was still plentiful haze left in the atmosphere, however. The second experiment day had a much drier atmosphere, with clear skies already present at dawn.

As can be seen from the two graphs in Figure 7, the clear water ratio between DMSC channels 3 and 2 was significantly greater (700) on Day 1 than on Day 2 (565). Very encouraging, however, was the fact that on both days the ratios corresponding to oil slicks of increasing thickness deviated similarly from the clear water relationship. Hence, while the ratio values themselves are relative and can vary due to background radiance and atmospheric effects, the absolute difference of the oil ratios from the measured background ratio appears to have robust correlation to the oil's thickness. The absolute

differences were used to calibrate our thickness algorithm and classify imagery from each sample area. A sample classification from one of the study sites is shown in Figure 8. Approximately half of the ship-based measurements were used to assess the algorithm's accuracy. The algorithm was found to have an error margin of 20-37%, depending on the site sampled. It must be noted, however, that due to the great heterogeneity of thickness patches within each slick on spatial scales that often approximated the image pixel size, some of the error was undoubtedly contributed to by slight spatial mismatching between the sample pixel(s) and the actual spot that the ship sample was drawn from. Additionally, the fuzzy ratio-based classification results in grouping the image pixels into thickness range classes (rather than attempting to compute a specific value for each pixel on a continuous scale). A more comprehensive error testing under more controlled conditions was planned for the Ohmsett experiments (see below).

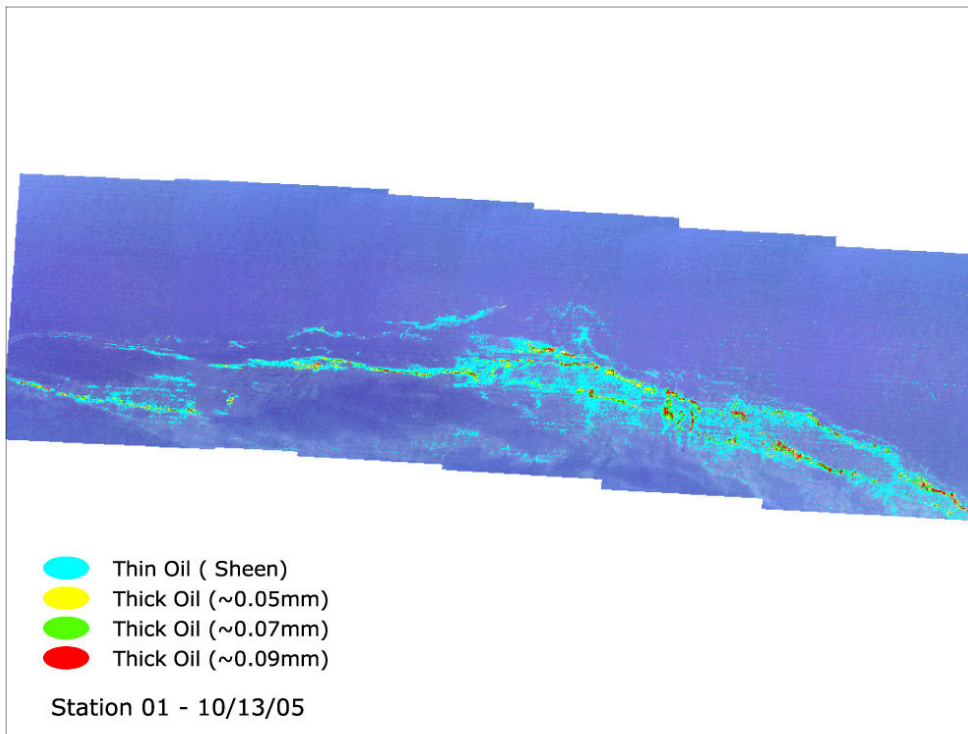
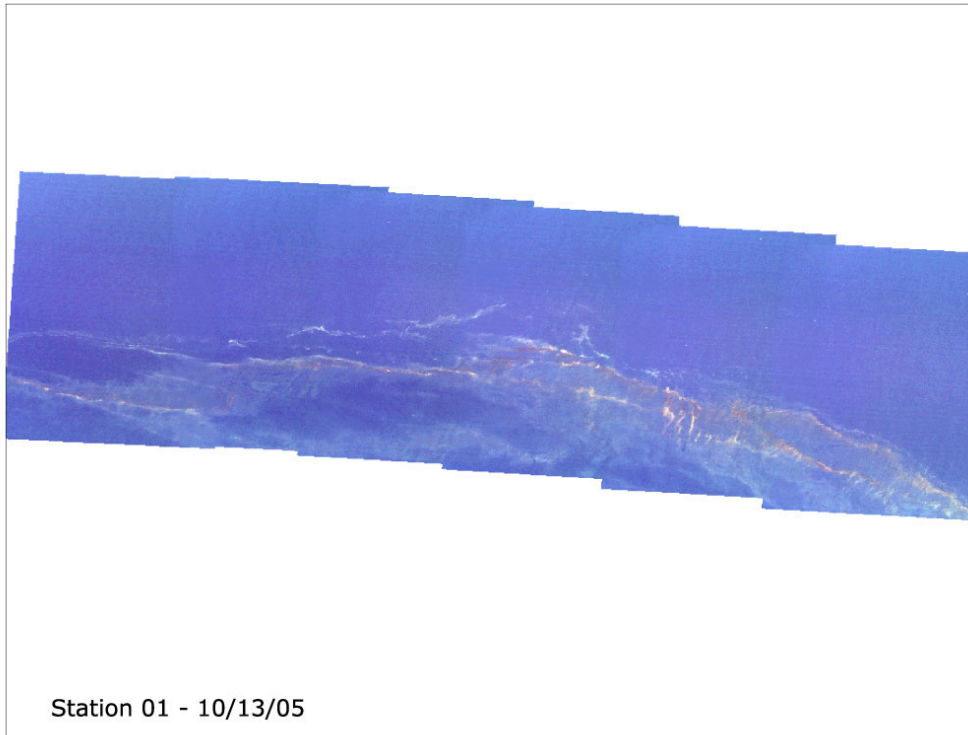


**Figure 7.** Membership functions derived through the fuzzy ratio classification algorithm for various oil thicknesses derived on Sampling Days 1 (left) and 2 (right).

One surprising finding during the field sampling was that the Santa Barbara seep slicks tend to be quite thin: we found films from unmeasurable thicknesses to a maximum of about 0.15mm. In a few cases the volume-per-area and theoretical thickness of emulsified film may have been greater, but we found it to contain about 50% water. Analysis of our DMSC imagery indicated that in none of the sites did thicknesses approach the upper measurement limit of our method. As was already mentioned above, that thickness was experimentally estimated at around 0.4-0.5mm for Monterey-type crudes.

The Santa Barbara Seep experiments proved that our thickness measurement algorithm approach is applicable in a real-world situation and allowed us to test its efficacy. It also provided us with data that were subsequently used to refine the algorithm software and running procedure. More information and images from the Santa Barbara experiments are contained on a DVD that was compiled and distributed to project participants earlier in the project and is included with this report.





**Figure 8.** Multi-frame mosaic of DMSC imagery over Site 2, Day 2. Original multispectral data (top) and resultant thickness classification (bottom).



### 3.4 Ohmsett Experiments

The original objectives of conducting tests in Ohmsett's tank were to validate the developed algorithm and archived oil signature files for the medium crude oil type, and to obtain new data for other crude and fuel oil types. For this reason the Ohmsett experiments were scheduled as the last task of the project. Although validation data were obtained, the Ohmsett work yielded new insights into oil reflectance properties and its behavior under larger-scale, more ocean-like conditions and waves. This, in turn, led to some modifications of the final algorithm and provided guidance for future refinement of the oil thickness measurement system.

#### 3.4.1 Experiment Design and Suggestions for Future Testing

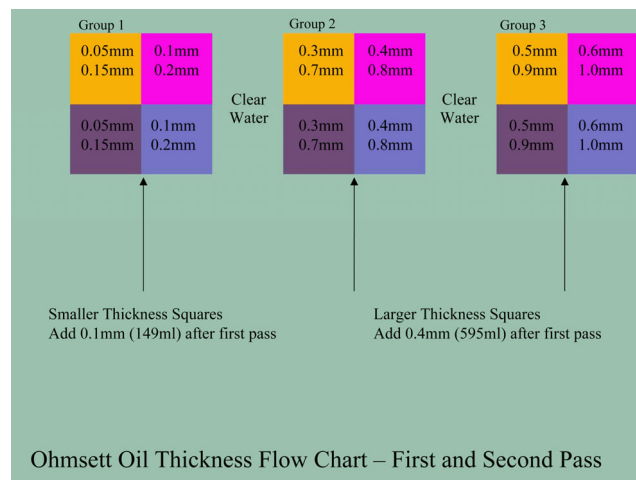
OI staff visited the Ohmsett facility first in March, 2006 to design appropriate camera mounting brackets and other logistics. The DMSC sensor was to be mounted atop a crow's nest above the tank's moving bridge (approximately 10m above water line), and was also to be mounted to a locally chartered helicopter for imaging the oil targets from higher altitudes, 300 – 600m. Both brackets were manufactured for us by Ohmsett personnel during the following month. They worked perfectly and are shown in Figure 9. If similar tests are done at Ohmsett in the future, the only change we would make is to attach the crow's nest mount to the north side of the platform. Although this will be slightly more difficult due to the platform's shape, the sensor will view the water surface away from the sun (since the sun arcs from east to west in the southern portion of the sky), thus minimizing sun glint which caused parts of the acquired imagery to be glint-contaminated in the south-viewing configuration.

The experiments were conducted during 16-19 May, 2006. 4" gray PVC piping, formerly obtained by the Ohmsett staff, was assembled by the OI, California Dept. of Fish and Game (CDFG) and Ohmsett crews into 12 1.3m squares, and these were then connected in groups of 4, separated by 1m gaps that served as "clear water" target areas. Different amounts of oil, corresponding to a desired oil film thickness when spread evenly within each square, were then poured from the bridge into the squares. Duplicate volumes (i.e. thicknesses) were used in each adjoining pair of squares for control purposes. From its position on the crow's nest, each DMSC image frame captured approximately one 4-square quadrant. The sensor was activated to capture 60% overlapping frames as the bridge traveled at approximately 0.5kt over the targets, and the entire target set was thus imaged with each pass. The experimental design is shown in Figure 10.

From earlier small-scale experiments with the various oils in OI's lab we were aware that a homogeneously thick film cannot be readily created by simply pouring oil into the confined area. This is especially true when trying to create films with thicknesses less



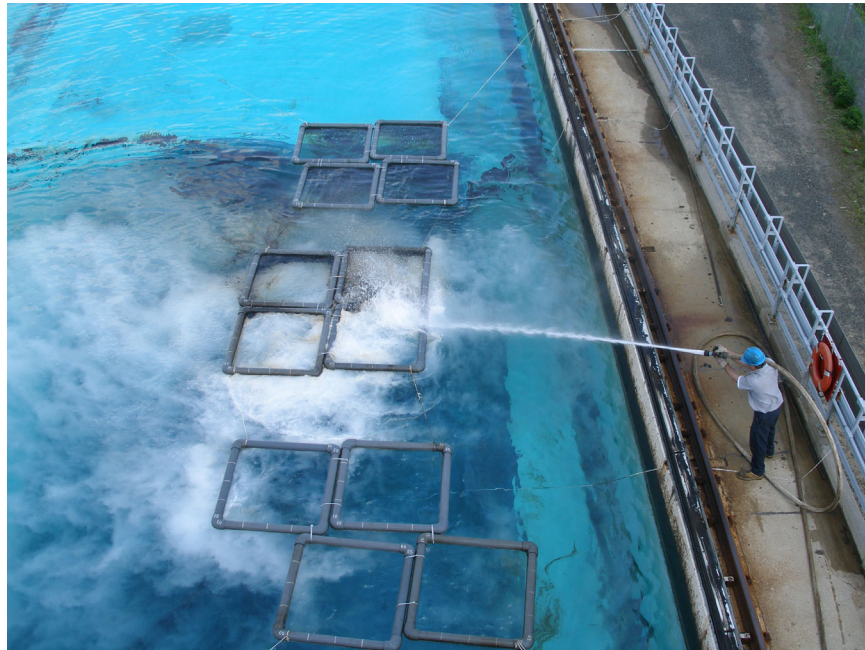
**Figure 9.** The DMSC imager mounted on Ohmsett tank’s crows nest (left) and on the skids of the helicopter (right).



**Figure 10.** Flow-chart of oil thickness films for each pass over the PVC square enclosures.

than 0.1mm. We finally settled on adding 7-10% (by volume) of turpentine to each oil sample, which greatly aided its spreading without significantly changing the film’s optical properties. The same procedure was used for the Ohmsett samples. In addition, after pouring the oil into each square, its spreading was aided by gently stirring or spreading it with a garden rake-like implement created by attaching a bundle of thin straight, stiff wires to the end of a boom. This procedure worked well, and once the oil was spread evenly throughout each square it tended to remain so for the duration of the experiment.

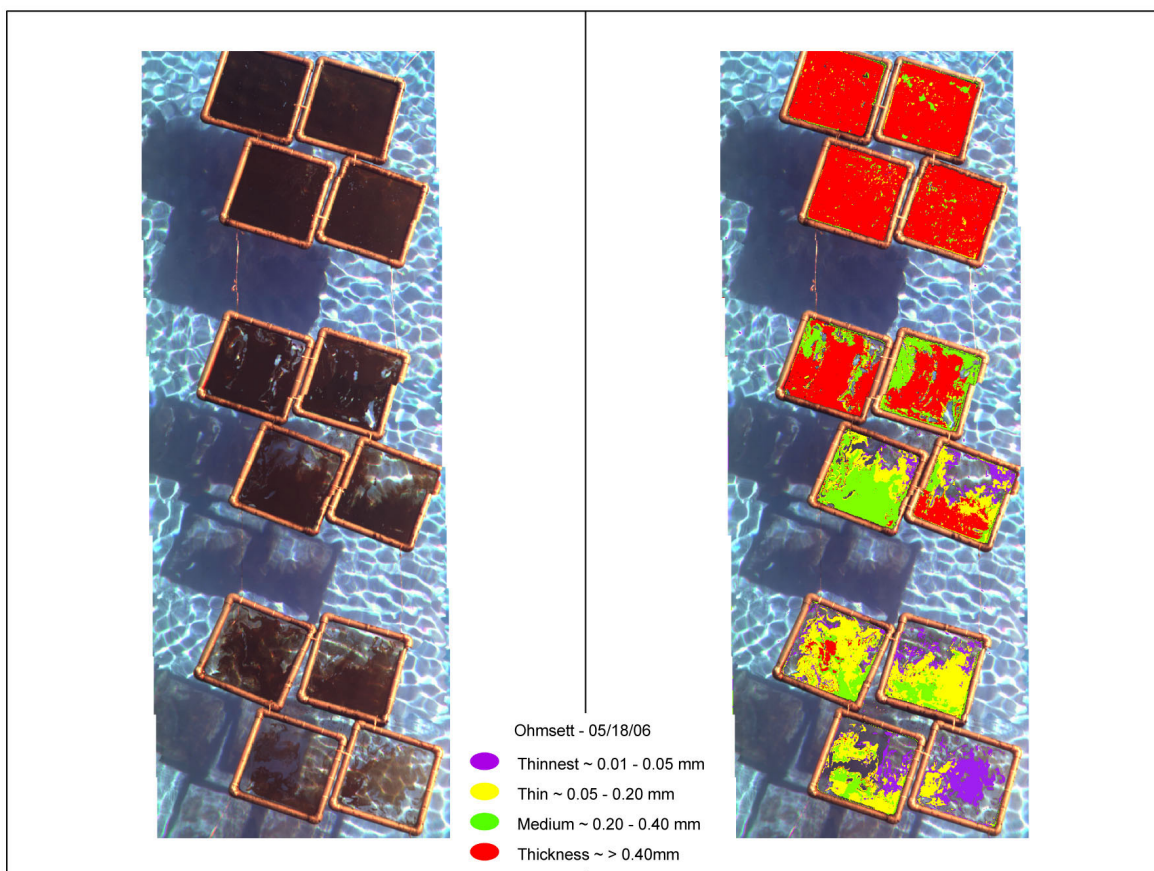
Once the entire square set was imaged, a second volume of oil was added to each to create increased film thicknesses (see Figure 10 ) and the entire set was imaged again. After the second pass all the squares were emptied and cleaned for the next experiment by high pressure flushing (Figure 11), which worked quickly and was very efficient.



**Figure 11.** Cleaning of the sampling squares with a high pressure hose.

One initial concern was that wind will push all or part of the spread oil film toward the lee side of each square, thus altering its thickness. This proved to be a problem in some instances, as can be seen in some of the oil enclosures shown in Figure 12. It could be minimized by acquiring imagery only while the bridge moved from north to south over the squares. Strong air convection between the bridge and the tank surface was apparently created when the bridge moved from south to north, creating major draft-caused effects within the squares.

Another concern that proved to be a greater hinderance was weather. Since the Ohmsett facility is heavily used, it must be reserved long in advance and last minute changes are not possible. The week of our experiments was quite rainy, with showers and thunderstorms occurring most of the days. With constantly variable cloudiness, “sunny” or “cloudy” data had to be quickly collected during windows of opportunity and even then the illumination conditions were generally not constant from sample set to sample set or from one day to the next. We believe the illumination variability was the greatest source of systematic error in the obtained data. (Although such variable conditions can be expected to sometimes occur in the field under operational circumstances, our purpose at Ohmsett was to acquire baseline characterizations for the different oils and conditions and constant background conditions were thus desired.)



**Figure 12.** True color view of sample squares containing different oil concentrations (left) and resultant thickness classification (right). Wind shear had affected the oil film homogeneity in the thin-film squares.

The Ohmsett tank's bottom and sides are white in color and its water depth is approximately 3m. Hence bottom reflectance was expected to cause major artifacts, since such strong reflectance is absent in real-world spills (except, perhaps, if a spill occurred over the shallow sand banks of the Bahamas or similar locale). To approximate the reflectance effects of deep water, a blue-green plastic tarp was submerged under the target squares and stretched over the bottom. This procedure seemed simple in principle at first but proved to be one of the most error-inducing aspects of the experimental setup. The tarp had two problems: First, it was neutrally buoyant. Although it could be weighed-down with pieces of metal and cinderblocks, the tank's slight current from its filtering mechanism and wind-caused water movement caused the tarp's sections between the weights to rise from the bottom. Second, the tarp material was slightly shiny. Under sunlight, the raised portions of the tarp created varied reflectance effects, depending on the angle of each tarp section. This created several different background (i.e. clear water approximation) conditions that had to be carefully evaluated and separated during data analysis so that valid computations and comparisons could be made. Nevertheless, the simulation of a non-white, deep water background is absolutely essential for any similar

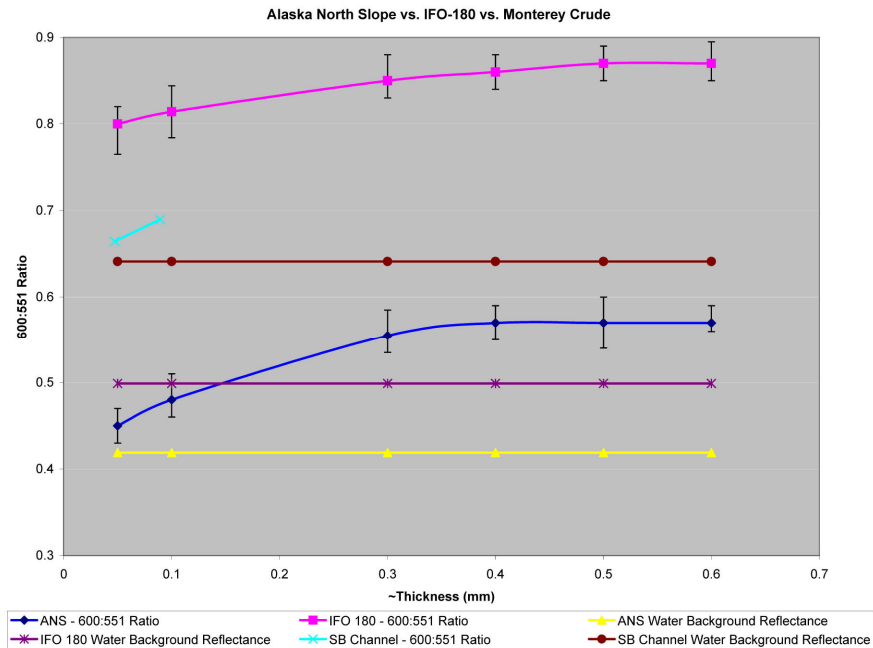


work in the future. We suggest the use of a non-plastic tarp, made from a non-shiny material such as died canvas, to which small but evenly distributed diver weights are attached before submerging it.

### 3.4.2 Experiment Results.

Most of our work was done using Alaska North Slope Crude (ANS), which we found in the lab to have very similar thickness-related spectral properties to Arabian Medium and Northstar oils. Figure 11 shows a multiframe mosaic of one of the ANS data sets, and a resulting thickness classification. Depending on the existing weather conditions, each data set was scanned several times to obtain multiple image samples for analysis.

Figure 13 summarizes the Ohmsett results for sunny conditions using the ratio of 600/551nm. Data from the Santa Barbara Channel seeps is also included although, as was discussed above, none of the sampled Santa Barbara slicks with fresh oil had thicknesses greater than approximately 0.1mm. For all the oil types the 600/551 ratio increases with increasing thickness, corroborating our earlier laboratory findings with Arabian Crude (see Figure 4). When the offset from the clear water background ratio is



**Figure 13.** Summary of results of thickness determinations using the 600/551nm ratio for multiple imaging passes with ANS (N=9) and IFO-180 (N=5) under sunny conditions. Only data with minimal surface and bottom tarp glint were used. Bars show range of all measurements, dots represent average value. Also shown are measurements from fresh oil in the Santa Barbara Channel.

considered, also as found previously, the offset increases with increasing thickness. This same general relationship was found to hold for both ANS and IFO-180 crudes. A marked difference in the offset-from-background exists between the oil types, however,

with the much thicker IFO-180 having greater offsets at all thicknesses tested. For example, at film thickness of 0.3mm the ANS offset is 0.056 while the IFO-180 offset is 0.18. (The reason for the two different water background values is due to differences in illumination and underwater tarp reflectance between the different times when the two oil samples were scanned.) The oil type-related offset differences show that, as was expected, different archived oil signature files must be created and the appropriate one (provided some information is available about the type of oil spilled) then chosen to guide the thickness algorithm.

As was already discussed, our previous lab experiments done in shallow containers supported the notion published by other researchers that a near-IR channel provides useful oil thickness determination information. We therefore included a near-IR channel in the initial DMSC configuration at Ohmsett, at the expense of a short-wave (e.g. 420nm) channel. With no upward bottom reflectance of the near-IR wavelengths in the deeper waters of the Ohmsett tank, the initially prepared algorithm that utilized band ratios using the near-IR band had to be modified. For that reason we show here thickness determinations based on the 600/551 ratio, which proved the most reliable. We expect these results to more closely resemble actual offshore conditions.

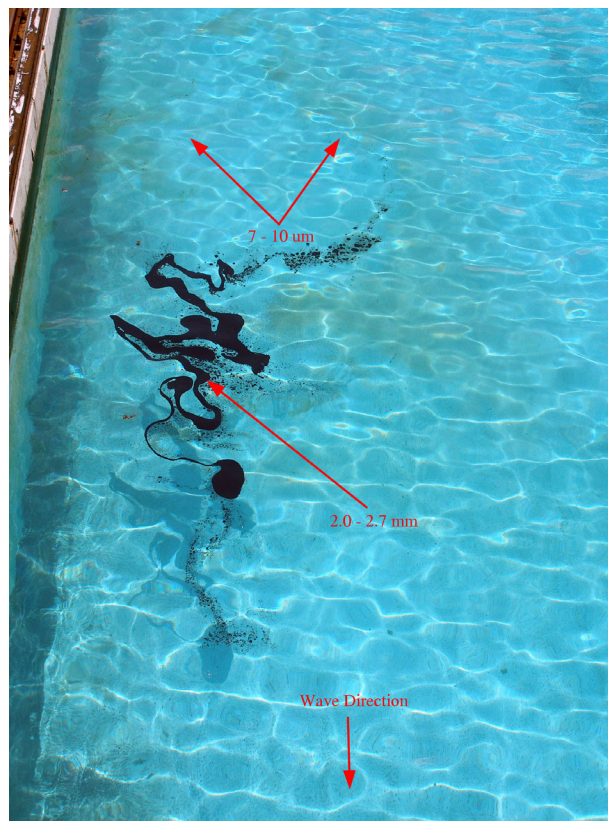
The results shown in Figure 13 also indicate that the maximum thickness that can be measured using strictly visible spectrum wavelengths is about 0.4mm for ANS and 0.3mm for the more viscous IFO-180. At greater thicknesses the film's reflectance characteristics no longer change significantly since sunlight no longer penetrates through the entire film. As we have suggested elsewhere, the addition of an IR channel to the imaging system could increase the thickness measurement range since heat radiance characteristics have been shown to be related to thickness, particularly from thicker films.

The data in Figure 13 include samples gathered from the crow's nest-mounted DMSC as well as one ANS sample set obtained at 1000 feet altitude from the helicopter-mounted sensor. No statistically significant difference was found between the crow's nest and helicopter samples. This is logical since the atmosphere was quite clear during the overflight and little atmospheric attenuation could thus be expected through the 1000 foot distance (the pilot could not go any higher at the time). It must be noted, however, that most of the helicopter-acquired data was heavily contaminated by sunglint and could thus not be used, since the flight was done much latter in the day (at 11:40am) than originally scheduled, resulting in a very high sun angle.

One other notable observation from the data in Figure 13 is the position of the Santa Barbara oil seep data on the ratio scale. Santa Barbara's Monterey crude is significantly heavier than ANS but not as heavy as the IFO fuel oil. Accordingly, the Santa Barbara data ratios fit between the other two oils tested at Ohmsett. There thus appears to be a consistency in the ratio-to-oil type relationship, with increasing ratio (and offset-from-background reflectance) values with increasing oil type viscosity.

On the last day of the Ohmsett experiments we released approximately 3 liters of each oil type into the tank outside the square enclosures, activated the wave generator at 30 cycles

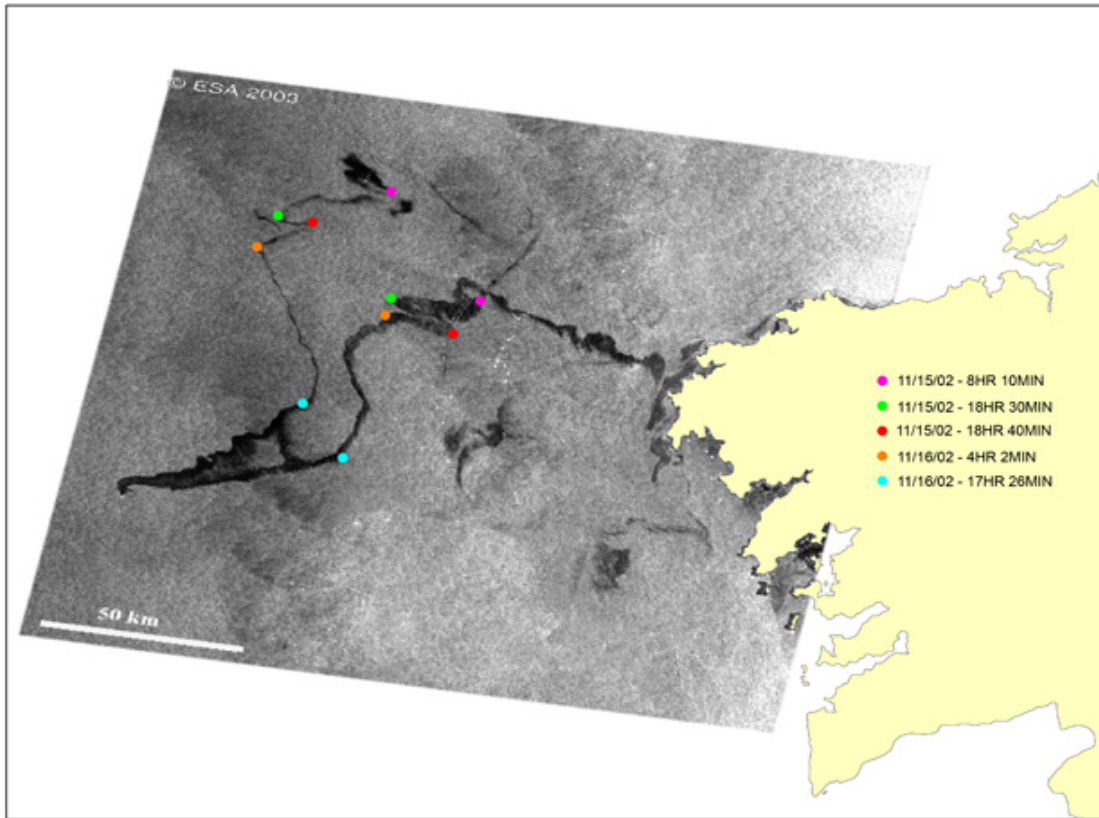
(substantial but not crest-breaking waves) and recorded the spreading/travel characteristics of each oil with time. The ANS tended to retain its greatest thicknesses in its leading-edge area, creating a trail of progressively thinner oil film and sheen. This behavior is logical, since the thickest slick components will absorb the most wave energy and will thus travel the fastest in the wave direction. The behavior of the IFO-180 sample was quite different: after a few minutes the initial slick separated into two distinct components, one with relatively thick patterns (terminal thickness was physically measured (by the same method as we used in the Santa Barbara Channel) as 2-2.7mm), the other consisting of an homogenous 7-10um thick film. As can be seen from Figure 14, after only 7 minutes the thicker portion of the slick had traveled a considerable distance from the thin portion. We suggest that this phenomenon is due to the relatively rapid separation of the less viscous, more volatile components of the fuel oil from its bulk. A spill of fuel oil on the open sea could thus in time result in two (or more) slicks with vastly different locations and drift rates, as well as thickness compositions.



**Figure 14.** Separation of thin (light brown) and thick (black) components of an IFO-180 slick after 7 minutes of 30 cycle waves.

A vivid real-world example of such a dual oil slick having formed during an actual spill can possibly be the satellite Synthetic Aperture Radar image in Figure 15. The image, captured in the morning of 17 November, 2002, shows oil slick patterns from the sinking tanker Prestige as it was being towed for several days by Spanish-directed tug boats. The

northernmost part of the slick is in the approximate location where the ship was maneuvered and resumed being towed on 11/15. During the two days until the image was captured the slick apparently split into two components, forming a distinct “V”. While its eastern portion retained most of the same shape and spatial pattern as its western counterpart, it traveled much more rapidly toward the southeast. The Prestige was leaking its cargo of heavy fuel oil (Russian 100) and we believe similar processes affected its slick as we observed in the Ohmsett tank with IFO-180.



**Figure 15.** ENVISAT satellite SAR image acquired on 11/17/2002 showing oil slicks from the leaking tanker Prestige off Spain. The color dots show the corresponding features within the slick which has separated into two components moving at different velocities due to wind, current and wave influences.



## **4. CONCLUSIONS**

Below are the most significant conclusions gained to-date from this project:

Oil film thickness in the range from sheen to approximately 0.5mm can indeed be measured over open water using a multi-channel UV-Vis aerial imaging sensor.

The oil thickness determination algorithm must account for basic optical differences in oil types (i.e. light-midweight crudes vs. heavy crudes and fuel oils), different background water color conditions and ambient light conditions (i.e. sunny vs. cloudy skies).

Near-IR wavelengths are not useful for oil thickness determination but aid in determining the weathering state of the floating oil.

Before operational application, additional calibration and error assessment testing of the developed system should be performed, with special attention to background illumination effects. Especially important is the testing of the transferability of the algorithm-leading parameters for a particular oil type from one set of oceanic conditions to another. Ideally, “real-world” tests on the open sea would provide the most realistic assessment of the algorithm’s reliability.

## **5. RECOMMENDATIONS**

Based on the results obtained through this project it now appears that a portable oil slick thickness mapping system based on an aerial multispectral sensor can be developed for fully operational use in a relatively short time. To reach this final goal, we recommend that the following work be performed:

Improve the oil thickness classification software’s efficiency and automation to allow more rapid generation (and hence dissemination) of the oil distribution map products.

Enlarge the thickness algorithm’s oil type signature library to include oil types not tested in this project. This also needs to include signatures of the same oils under cloudy vs. sunny skies, since clouds especially tend to attenuate the longer wavelengths. Although some such data was obtained during this project, the vast majority of the results were obtained only under sunny conditions.

Investigate the addition of an Infrared (IR) camera to the system to extend the measurable thickness range past 0.5mm and, possibly, provide some measurement capabilities at night. Precedent investigations by European researchers have shown that IR imagery can be used to estimate oil thickness, with best capabilities over relatively thick areas (8, 13).

Perform more validation test to provide quantitative measures of the system’s achievable measurement accuracy. Although this project provided some accuracy validation results

from the Santa Barbara Channel experiments (RMS error at the 4 sites ranged from 20% to 37%), more strictly controlled accuracy assessments are needed for the final algorithm. Ideally, one part of such assessments could be a real-world open ocean experiment, as is sometimes done by the Europeans, with a known amount of oil released offshore. After imaging the created oil slick the total volume could be computed from the classified thicknesses within it, and the figure compared to the known total release amount. This would be the most convincing test of the developed system's utility in a real spill situation.

## 6. REFERENCES

- 1) Zielinski, O. 2003, Airborne Pollution Surveillance Using Multi-Sensor Systems. *Sea Technology*, Oct. 2003, 28-32.
- 2) Huhnerfuss, H., W. Alpers, H. Dannhauer, M. Gade, P.A. Lange, V. Neumann and V. Wisman. 1996. Natural and man-made sea slicks in the North Sea investigated by a helicopter-borne 5-frequency radar scatterometer. *Int. J. Remote Sensing*, 17(8), 1567-1582.
- 3) Gade, M., W. Alpers, H. Huhnerfuss, H. Masuko and T. Kobayashi. 1998. Imaging of biogenic and anthropogenic films by the multifrequency/multipolarization SIR-C/X-SAR. *J. Geophys. Res.* 103(C9), 18,851-18,866.
- 4) Ausseil, J.D and J.P. Monchalain. 1989. Laser-ultrasonic measurement of oil thickness on water from aircraft. Feasibility study. *Industriql Materials Research Institute Report*. Boucherville, Quebec.
- 5) Chouquet, M., R. Hedon, G. Vaudreuil, J-P. Monchalain, C. Padioleau and R.H. Goodman. 1993. Remote thickness measurement of oil slicks on water by laser ultrasonics, In: *Proceedings of the 1993 International Oil Spill Conference*. American Petroleum Institute, Washington DC, 531-536.
- 6) Brown, C.E., M.F. Fingas, R.H. Goodman, J.V. Mullin, M. Choquet and J-P. Monchalain. 2000. Progress in achieving airborne oil slick thickness measurement. In: *Proceedings of the 23<sup>rd</sup> Arctic and Marine Oil Spill Program Technical Seminar*, Environ. Canada, Ottawa, Ontario, 493-498.
- 7) Piskozub J., V. Drozdowska and V. Varlamov. 1997. A LIDAR system for remote measurement of oil film thickness on sea surface. In: *Proc. Of the 4<sup>th</sup> Thematic Conference on Remote Sensing for Marine and Coastal Environments*, vol. 1, ERIM, Ann Arbor, Michigan, 386-391.
- 8) Byfield, V. 1998. *Optical Remote Sensing of Oil in the Marine Environment*. PhD Thesis, U. of Southampton, School of Ocean and Earth Science.
- 9) Rogne T., I. Macdonald, A. Smith, M.C. Kennicutt, and C. Giammova. 1993. Multispectral remote sensing and truth data from the Tenyo-Maru oil spill. *Photogr. Engin. and Remote Sensing*, 59(3), 391-397.
- 10) Alhinai K.G., M.A. Khan, A.E. Dabbagh and T.Bader. 1993. Analysis of Landsat Thematic Mapper data for mapping oil slick concentrations – Arabian Gulf Oil-Spill 1991. *Arabian J. for Science and Engineering*, Vol. 18(2), 85-93.
- 11) Gillot, A., G.H.R. Aston, P. Bonanzinga, Y. le Gal la Salle, M.J. Mason, M.J. O'Neill, J.K. Rudd and D.I. Stonor. 1988. Field guide to application of dispersants to oil spills. Rept No.2/88. The Hague, Netherlands, CONCAWE. 64pp.
- 12) Lennon, M., S. Babichenko, N. Thomas, V. Mariette, G. Mercier, and A. Lisin. 2006. Detection and Mapping of Oil Slicks in the Sea by Combined Use of Hyperspectral Imagery and Laser Induced Fluorescence. *EARSel eProceedings 5, Issue/2006*, 1-9.
- 13) Davies L., J. Corps, T. Lunel and K. Dooley. 1999. Estimation of oil thickness. *AEA Technology*. AEAT-5279(1). 1-34.

## **APPENDIX A**

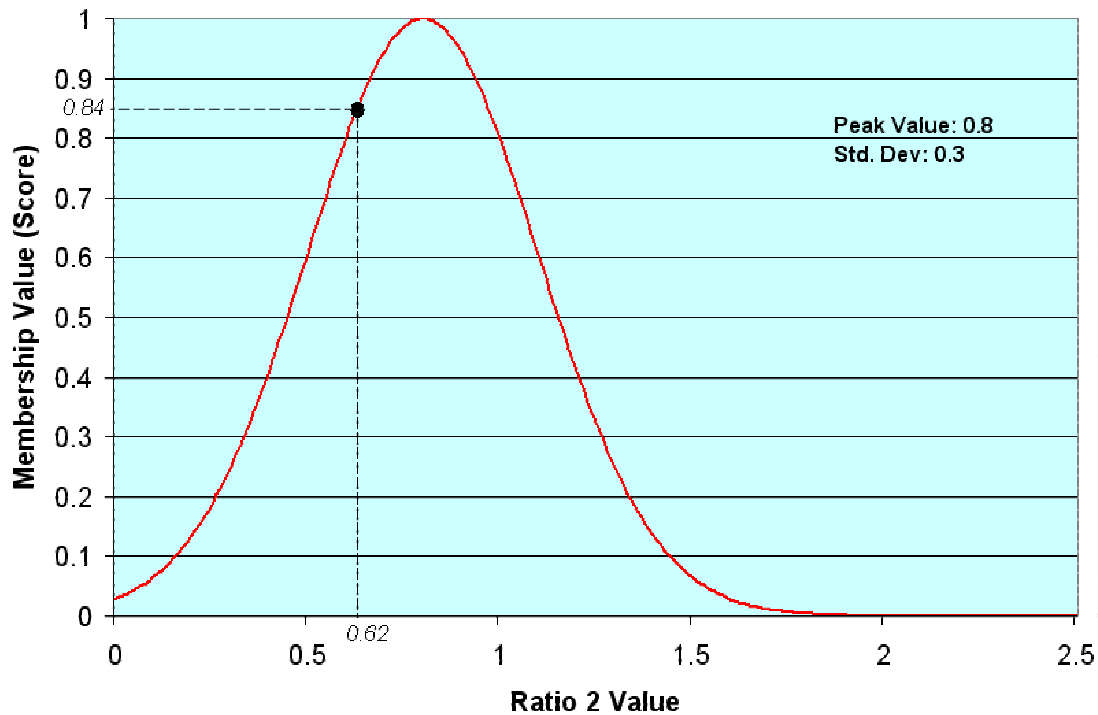
### **Oil Thickness Algorithm Software Details**

# Fuzzy Ratio Based Classification in OI Imaging Tools

An Introduction to Fuzzy Classification.

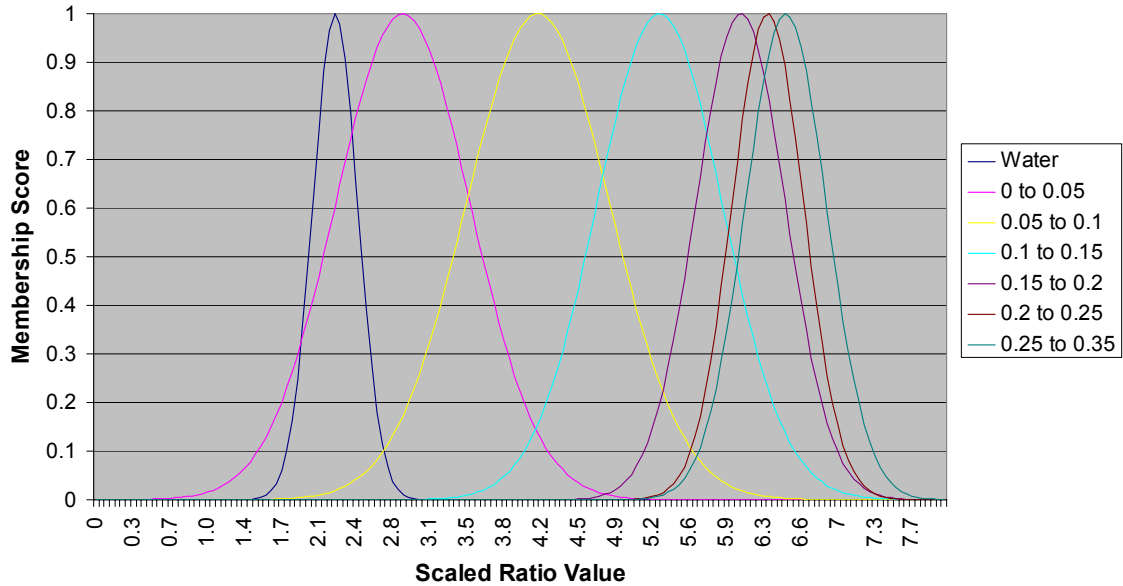
The basis of a fuzzy classification is a collection of pre-determined membership functions for the desired classes (i.e. water, grass, pavement) and attributes (i.e. band 4/band 3 ratio, band 2 DN, etc.). Each class definition consists of one membership function for each of the desired attributes. In OI Imaging Tools, a membership function takes the form of a bell curve. The X-Axis is the value of the attribute in question, and the Y-Axis is the *membership score*. A membership score is a measure of how likely a specific sample (pixel) is a member of a class. The graphic below shows a hypothetical membership function corresponding to “Class 1” for the “Ratio 2” attribute. The curve shows that if a pixel is a member of class 1, it is expected to have a ratio 2 value of about 0.8. At a ratio value of 0.8, a pixel would receive the highest possible membership score

**Class 1 Membership Function (Ratio 2)**



of 1.0. The graph shows a hypothetical pixel with a ratio 2 value of 0.62. This corresponds to a membership score of 0.84. The membership function quickly drops to zero, so pixels with values far away from the peak will receive a membership score of zero, indicating it is impossible for the pixel to be a member of the class.

### Membership Curves, 4:3 Ratios - 3/16/06



In a classification with many classes, there will be many membership functions. The following graphic shows a collection of membership curves for oil thickness classes based on a 4:3 band ratio. As the graph shows, membership functions can vary in shape. A wide membership function for a class means that the class includes a wider variety of values for that attribute. A narrow membership function corresponds to a class with little variation for the specified attribute. It is also possible for membership functions to overlap. This makes it possible for a pixel to have a membership scores for several classes at once.

Each pixel is scored by the membership functions of each class and attribute. These scores are then analyzed to determine how the pixel will be classified. The table below shows the membership scores for a hypothetical pixel in an oil slick thickness

Class	Membership Value (Score)			
	4/3 Ratio	4/2 Ratio	4/1 Ratio	Min Score
<b>Clear Water</b>	0	0	0	0
<b>0.01mm to 0.05mm</b>	0	0	0	0
<b>0.05mm to 0.1mm</b>	0	0.2	0.2	0
<b>0.1mm to 0.15mm</b>	0.2	0.3	0.4	0.2
<b>0.15mm to 0.2mm</b>	0.3	0.4	0.8	0.3
<b>0.2mm to 0.25mm</b>	<b>0.9</b>	<b>0.7</b>	<b>0.75</b>	<b>0.7</b>
<b>0.25mm to 0.35mm</b>	0.35	0.4	0.3	0.3
<b>0.35mm to 0.45mm</b>	0	0	0.25	0
<b>0.45mm to 0.55mm</b>	0.2	0.5	0.1	0.1
<b>0.55mm to 0.65mm</b>	0.7	0.1	0	0

classification. The first Column of the table lists the class names, while the top row lists the attribute for which the membership score is calculated. For instance, in the 0.1mm to 0.15mm class, the sample pixel received a score of 0.2 for the 4/3 Ratio membership function, a score of 0.3 for the 4/2 Ratio membership function, and a score of 0.4 for the 4/1 ratio membership function. These 3 scores are then used to create a total score for this class for this pixel. This is done by taking the minimum of the three scores. It may seem more intuitive to just average the scores, but this can lead to errors. If a pixel were to get a very high score for two of the ratios and a zero for the third, this pixel is not a member of the class since the third ratio was nowhere near where it should be. Taking the minimum score yields a 0, but taking a mean would yield a misleading higher score. Once the minimum score is computed for each class (as shown in the last column of the table), the pixel is declared to be a member of the class with the highest minimum score. In this case, class “0.2mm to 0.25mm” with a membership score of 0.7. A threshold may be implemented here such that if no class had a score higher than a certain value, say 0.1, the pixel will be declared “Unclassified” since it didn’t fit any class very well.

## Carrying out a Fuzzy Ratio Based Classification in OI Imaging Tools



Because a fuzzy ratio-based classification is a supervised classification, the first step is the creation of a training set.

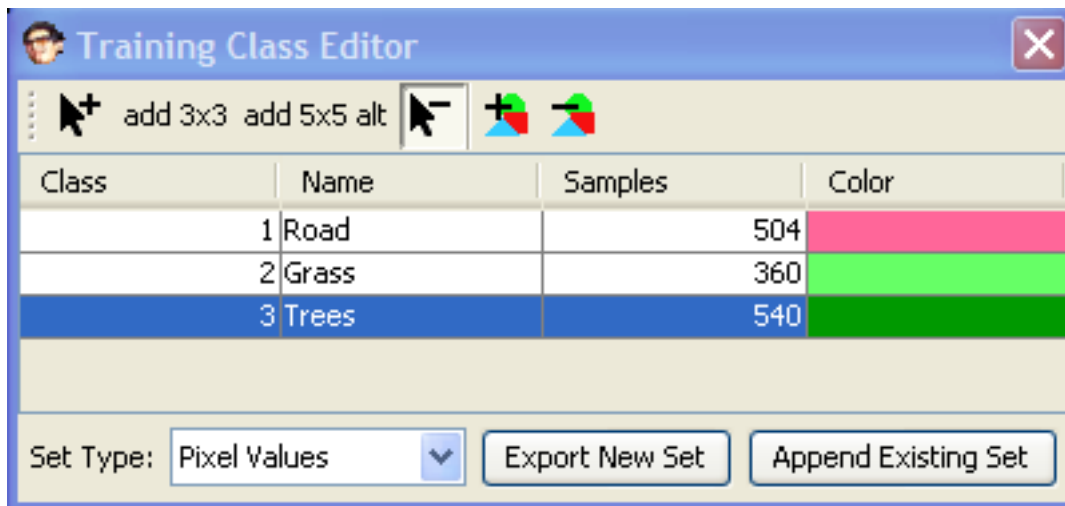
(The following instructions are the same as the instructions for creating a Neural Network training set through step 6. Step 7 if different)


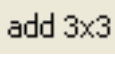
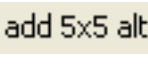

### Creating a Training Set

Training Sets are created just as they are for any type of supervised classification. However, there are a few tips for creating a training set that will be optimal for a neural network.

To create a training set:

1. Open the image to be used for generating the training set.
2. Select *Classification -> Create Training Set* from the main menu. The Training Class Editor Dialog will appear. Note: this dialog is only intended to be used with the image that was selected while the dialog was opened.
3. Click the Add Class Button  repeatedly until the desired number of classes has been added. (Classes may be deleted from the class table by selecting the row in the table and clicking the Delete Class Button .)
4. Click on the cells of the class table to change the class names and colors.
5. Select the class you would like to add samples to by clicking its row in the class table so it is highlighted blue.

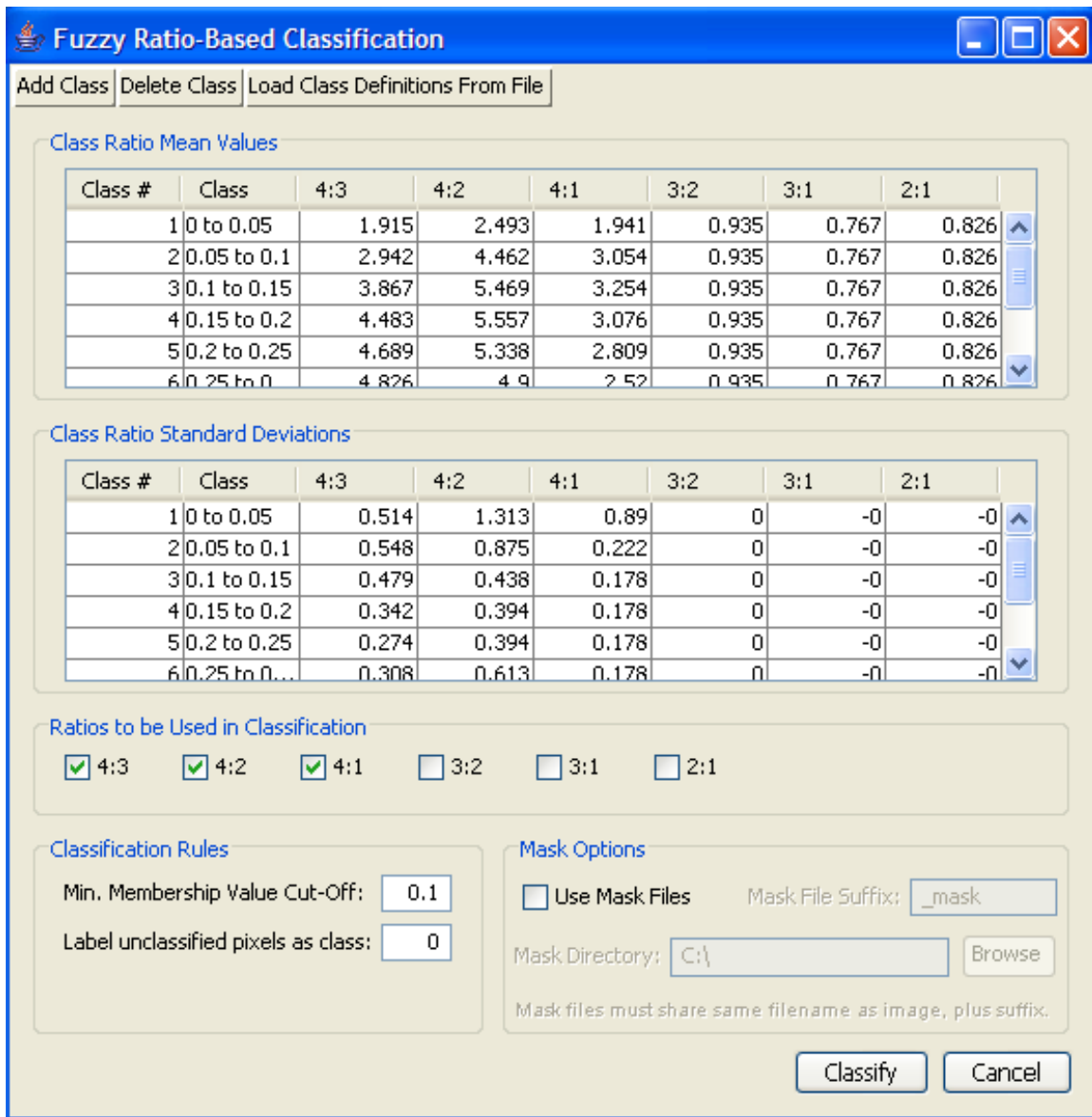


6. Add samples (pixels) to the selected class with the assorted tools:
  - a. Add Pixel Tool  adds one pixel at a time with single clicks on the image, or a group of pixels by holding down the mouse button and drawing a rectangle around the desired pixels.
  - b. Add 3x3 Tool  adds a 3x3 square of pixels (9 pixels) centered on the pixel clicked.
  - c. Add 5x5 Alt Tool  adds a 5x5 square of pixels alternating in a checkerboard pattern (12 or 13 pixels) centered on the pixel clicked.
  - d. Delete Pixel Tool  deletes one pixel at a time with single clicks on the image, or a group of pixels by holding down the mouse button and drawing a rectangle around the pixels to be deleted.
  
7. Once the training set is complete, it must be saved to file. For a fuzzy ratio-based training set, the **“Set Type:” drop-down list MUST BE SET TO “Class Ratio Stats”**. This training set can be saved as an individual training set by clicking the “Export New Set” button, or it may be appended to an existing Pixel Values training set file by clicking the “Append Existing Set” button. When a large area composed of many image frames is being classified, it is advisable to create training sets from several sample images and combine them into one training set by appending them to each other. When appending a training set a dialog will appear to match

## Classifying Images

Once the training set has been created select *Classification -> Fuzzy Ratio-Based Classification* from the menu. A dialog will appear. This dialog allows the manual creation of classes by clicking on the “Add Class” button and manually entering the mean

and standard deviation values for each ratio for each class. However, if a training set has been created, all of this information has already been calculated and stored in the training set. Click the “Load Class Definitions From File” button and select the training set.



- The Class Ratio Means table contains the mean values of each ratio for each class. The mean value is the location of the center of the membership curve (the highest scoring point).
- The Class Ratio Standard Deviations Table contains the standard deviations of each ratio for each class. The standard deviations are used to determine the width of the membership curves.
- The “Ratios to be Used in Classification” panel contains checkboxes stating which ratios to be used in the classification. Membership functions will only be generated for these ratios, the other ratios will be ignored



- The Minimum Membership Value Cut-Off is the threshold for classifying a pixel. If a pixel's maximum class membership score is below this level, the pixel will be considered unclassified.
- Unclassified pixels will be assigned the class number specified
- A mask file may be generated from a 2-class neural network classification. Masked pixels will not be considered for classification and will be noted as "Unclassified"

Once all the parameters are set, click "Classify" and choose the images to classify with this process.

## Oil Thickness Classification with OI Imaging Tools

The oil thickness classification procedure in OI Imaging Tools uses a fuzzy ratio-based classification. The procedure is the same as the fuzzy ratio-based classification instructions, except that the process is semi-supervised instead of fully supervised.

Instead of creating a training set with all the desired oil thickness classes, only a simple training set of a water class and an oil class is needed. The individual oil thickness class statistics are determined from the single oil class, and prior knowledge about the oil, stored in an oil signature file.

### Process for executing Oil Thickness Classification in OI Imaging Tools.

1. Create a training set as specified in the directions for a fuzzy ratio-based classification. The training set should contain two classes, Oil and clear water. **This training set must be saved as a “Class Ratio Values” training set, NOT a “Class Ratio Statistics” training set.**
2. Select *Classification ->Generate Oil Membership Functions*. This will display the “Generate Oil Membership Functions” dialog.
3. Click the “Browse Button” in the “Choose Ratio Training Set” panel. Select the Class Ratio Values training file created in step 1.

The screenshot shows the "Generate Oil Membership Functions" dialog box. It features a blue title bar with the text "Generate Oil Membership Functions" and standard window control buttons (minimize, maximize, close). The dialog is divided into three main sections, each with a blue header:

- Choose Ratio Training Set:** Contains a text box with "C:\", a "Browse" button, a "Select Clear Water Class:" dropdown menu, a "Select Oil Class:" dropdown menu, and a "Percentile to be considered maximum value:" text box with the value "90".
- Oil Signature File:** Contains a text box with "C:\", a "Browse" button.
- Output Membership Statistics:** Contains a text box with "C:\", a "Browse" button.

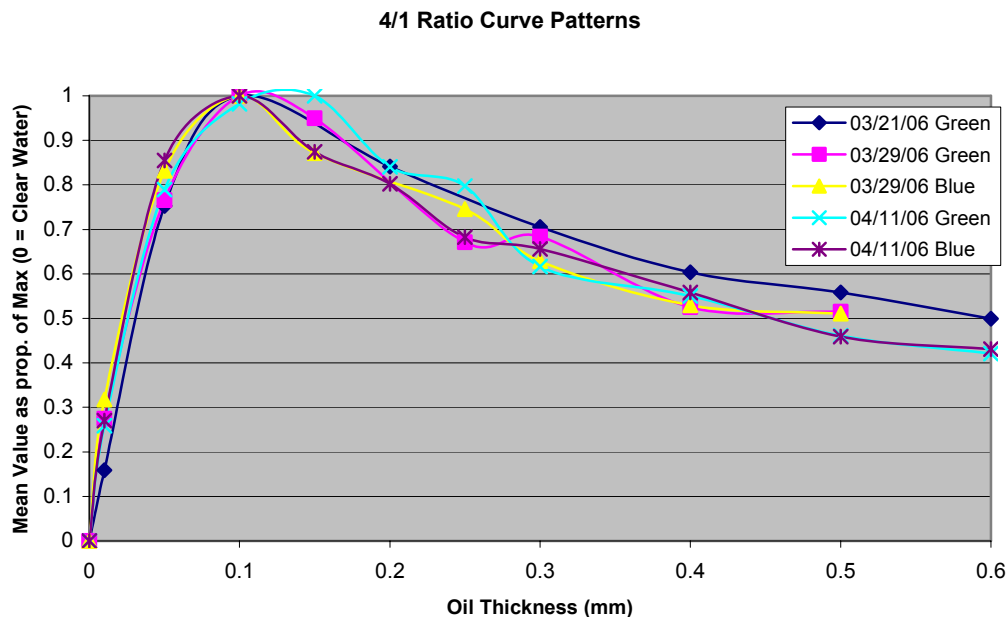
At the bottom of the dialog, there are two buttons: "Generate Membership Curves" and "Cancel".

4. Once the training set is loaded, the “Select Clear Water” and “Select Oil Class” drop-down lists will be enabled and populated with the classes from the training set. Choose the appropriate class in each list.
5. Enter the percentile to be considered the maximum value in the oil classes. The actual maximum value is not used to avoid outlier values skewing the results. It is suggested the the 90<sup>th</sup> or 95<sup>th</sup> percentile be considered the maximum value
6. Select the appropriate Oil Signature File.
7. Choose an output file for the generated class membership statistics file. This file will be in the format of a Class Ratio Statistics training set.
8. Proceed with a normal fuzzy ratio-based classification, using the newly created Class Ratio Statistics file to define the membership functions.

## Creating an Oil Signature File

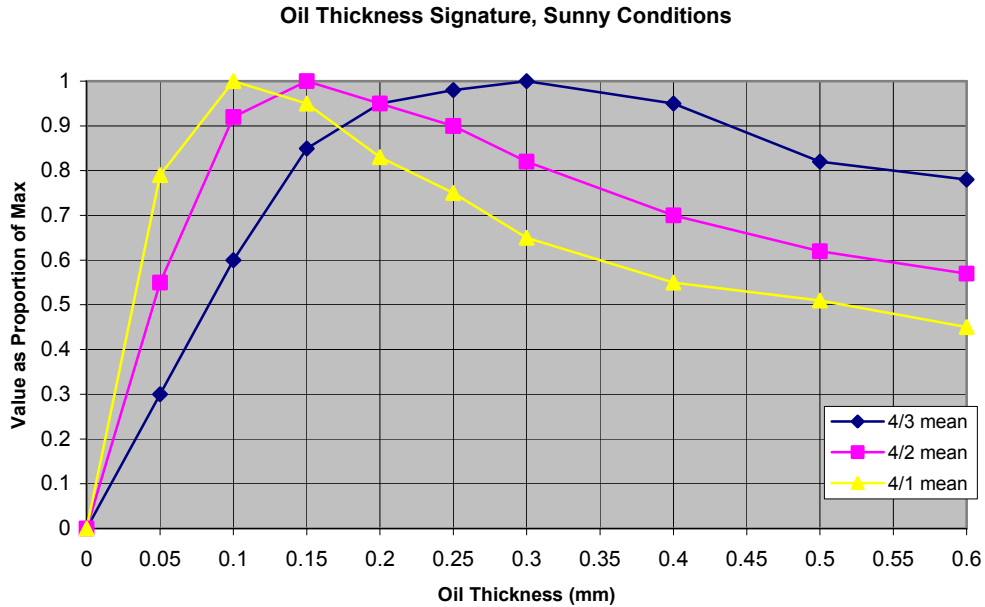
An oil signature file contains information about the behavior of oil ratios at different thickness classes. It is derived experimentally.

1. Generate graphs showing the ratio values for different oil thickness from multiple experiments.
2. While the ratio values themselves may change, it is assumed that the shape of the curve remains the same, with the maximum value corresponding to the same thickness.
3. To compare normalize these graphs, calculate the average water ratio values, and subtract it from all the data points, this should shift the graph down so it



nearly passes through the origin. Next, divide each data value by the maximum ratio value, this will rescale the curve between 0 and 1. Develop a graph for each desired ratio.

- Aggregate the lines in these graphs to derive one chart with one curve for each desired ratio.



- From this graph, choose class boundaries (i.e. 0.2 to 0.3 mm). For each class, determine the mean value of each ratio, as well as half the range for that value. (The range will be treated like the standard deviation). For example, in the graph above, for the class 0.2mm to 0.3mm, the mean value of the 4/1 ratio is 0.75, while half the range is approximately 0.1.
- Create a text file from these values in the following format:

The first line of the file should start with a # to denote it as a comment. This is the column headers, the columns should be class name, class means in descending ratio order, class StdDevs (half range) in descending ratio order:

**#Class Name,4/3 mean,4/2 mean,4/1 mean,3/2 mean,3/1 mean,2/1 mean,4/3 StdDev,4/2 StdDev,4/1 StdDev,3/2 StdDev,3/1 StdDev,2/1 StdDev**

The following should be one line for each class, with values in the order of the column headers. Do not include any spaces, and do not include extra returns after the last line:

**water,0.0,0.0,0.0,0.0,0.0,0.0,0.0,0.05,0.1,0.1,0.0,0.0,0.0  
 0 to 0.05,0.15,0.27,0.39,0,0,0,0.15,0.3,0.4,0,0,0  
 0.05 to 0.1,0.45,0.72,0.89,0,0,0,0.16,0.2,0.1,0,0,0**

**0.1 to 0.15,0.72,0.95,0.98,0,0,0,0.14,0.1,0.08,0,0,0**  
**0.15 to 0.2,0.9,0.97,0.9,0,0,0,0.1,0.09,0.08,0,0,0**  
**0.2 to 0.25,0.96,0.92,0.78,0,0,0,0.08,0.09,0.08,0,0,0**  
**0.25 to 0.35,1,0.82,0.65,0,0,0,0.09,0.14,0.08,0,0,0**  
**0.35 to 0.45,0.95,0.7,0.55,0,0,0,0.1,0.1,0.1,0,0,0**  
**0.45 to 0.55,0.82,0.62,0.51,0,0,0,0.08,0.08,0.08,0,0,0**  
**0.55 to 0.65,0.78,0.58,0.45,0,0,0,0.08,0.08,0.08,0,0,0**